analytical chemistry

Article

pubs.acs.org/ac

Two-Dimensional Continuous Extraction in Multiphase Lipid Bilayers To Separate, Enrich, and Sort Membrane-Bound Species

Ling Chao,[†,‡] Mark J. Richards,[†] Chih-Yun Hsia, and Susan Daniel*

School of Chemical and Biomolecular Engineering, Cornell University, 120 Olin Hall, Ithaca, New York 14853, United States

Supporting Information

ABSTRACT: A new method is presented to separate, enrich, and sort membrane-bound biomolecules based on their affinity for different coexisting lipid phases in a supported lipid bilayer using a two-dimensional, continuous extraction procedure. Analogous to classic liquid–liquid phase extraction, we created two distinct lipid phases in our planar membrane system: a liquid-ordered (l_o) phase and a liquid-disordered (l_d) phase arranged in parallel stripes inside a microfluidic device. Membrane-bound biomolecules in an adjacent supported lipid bilayer are convected in plane along the microfluidic channel and brought into contact with a different lipid phase using hydrodynamic force. A mixture of two lipid species, a glycolipid and a phospholipid, with known affinities for the two lipid phases employed here are used to demonstrate continuous extraction of the lipid-microdomain preferring glycolipid to the l_o phase, while the phospholipid remains primarily in the l_d phase. In this demonstration, we characterize the performance of this affinity-based separation device by building models to describe the velocity profile and transport in the two-phase coexistent membrane. We then characterize the impact of residence time on the extraction yield of each species. This new procedure sorts membrane species on the basis of chemical properties and affinities for specific lipid phases within a membrane environment near physiological conditions, critical for extending this method to the separation of lipid-linked proteins and transmembrane proteins while minimizing denaturation. This platform could facilitate the separation and identification of lipid membrane domain residents, or the characterization of changes in membrane affinity due to post-translational modifications or environmental conditions.

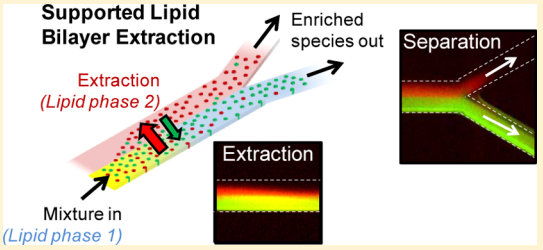

Membrane proteins and glycolipids are targets for therapeutic development,[1] but processing membrane-bound species while maintaining intact structural information, proper orientation, and necessary lipid associations remains a large bottleneck to characterizing and understanding their structure–function behavior.[2,3] The problem stems from the requirement of protecting the hydrophobic regions from water during processing. Many purification strategies use denaturing chemicals or conditions to remove species from the membrane and then use techniques developed mainly for soluble species to isolate them.[4,5] This approach can cause denaturation (in the case of proteins), disrupt orientational order necessary for binding to soluble species, and interrupt critical lipid associations (e.g., lipid microdomains) that are important for function.[6,7] Therefore, additional steps are required to restore the native, active structures and lipid associations. New strategies for separating membrane species in a native-like environment (i.e., a lipid bilayer) near physiological conditions would be attractive alternatives for this class of biomolecules.

A supported lipid bilayer (SLB) platform can protect the hydrophobic regions of membrane species. SLBs are chemically tunable and maintain the mobility of the species residing within them, including lipids,[8] glycolipids,[9] lipid-linked proteins,[10] and even some transmembrane species.[11−13] The planar geometry of SLBs facilitates the integration of surface analytical techniques that can be used to monitor lipid–lipid, protein–protein, or lipid–protein interactions, such as fluorescence microscopy,[14,15] ellipsometry,[16] and atomic force microscopy.[17−20]

Previous studies demonstrate the separation of membrane-bound biomolecules within supported lipid bilayers using electrophoresis,[8,21−24] bilayer self-spreading,[25] or bulk hydrodynamic drag.[26,27] However, these studies used SLBs of homogeneous chemical composition as the separation medium, so the separation was based solely on differences in biomolecule charge and/or mobility through the bilayer medium. None of these strategies separate species on the basis of their affinity for a specific lipid chemistry/environment.

Herein, we describe a planar (2-D) extraction platform that uses a two-phase coexistent SLB to separate membrane species based on their different chemical affinities for chemically distinct phases in the bilayer. This strategy is suited to this class of biomolecules because of the natural tendency of membrane-bound species to associate with different lipid phases in the cell membrane, such as glycolipids,[28] GPI-linked lipids,[29] and certain proteins.[30] These species tend to associate with lipid microdomains known as lipid rafts. Other membrane constituents tend to avoid lipid rafts and reside in more disordered phases enriched with phospholipids.[31] We exploit this natural partitioning tendency to carry out a two-dimensional extraction process in a planar SLB platform. To do so, different phases in the SLB

Received: February 20, 2013
Accepted: June 18, 2013
Published: June 18, 2013

   dx.doi.org/10.1021/ac4006952 | Anal. Chem. 2013, 85, 6696−6702

(i.e., membrane heterogeneity) must be constructed and patterned in a useful geometrical shape that facilitates the physical separation and sorting of species. Many studies have shown that coexistent liquid-ordered and liquid-disordered lipid phases can exist in model membrane systems,[14,19,20,32−34] but controlling the location of these phases has been a challenge. Recently we described a way to pattern stable phases in an SLB using laminar flow in a microfluidic device for the purpose of measuring partitioning kinetics of membrane-bound species to various lipid phases.[35] These partitioning rates were necessary parameters to measure for the current separation studies we present here. Here, we build upon this platform to perform 2-D extractions in planar membranes, characterize the separation and yield (enrichment) of membrane species to the different lipid phases, and develop a transport model for membrane-bound species in these two-phase bilayers.

EXPERIMENTAL SECTION

Materials. A detailed list of materials and suppliers is provided in the Supporting Information. Here we provide a brief list of the materials used in this work. Lipids used to make bilayers were 1-palmitoyl-2-oleoyl-sn-glycero-3-phosphocholine (POPC), ovine wool cholesterol (Chol), and 16:0 *N*-palmitoyl-D-erythro-sphingosylphosphorylcholine (PSM). Two lipids were used as extraction targets: *N*-(4,4-difluoro-5,7-dimethyl-4-bora-3*a*,4*a*-diaza-*s*-indacene-3-propionyl)-1,2-dihexadecanoyl-*sn*-glycero-3-phosphoethanolamine, triethylammonium salt (BODIPY FL DHPE), denoted as BODIPY DHPE in this work; and bovine brain asialoganglioside-G_{M1} labeled with Alexa Fluor 594 hydrazide, denoted as Alexa 594-G_{M1}.

Methods. A detailed description of the methods used in this work is provided in the Supporting Information. This includes our experimental setup; image processing methods; selection of stable heterogeneous lipid phases; liposome formation; microfluidic device fabrication; patterning procedures for the coexistent bilayers; two-phase bilayer stability controls; velocity profile determination in two-phase bilayer; and control experiments.

Simulation. A convection-diffusion model was constructed using COMSOL Multiphysics to simulate the transport of membrane species in the extraction device. Parameters for the model were obtained from the literature or independent experiments, as will be described in detail in the Results and Discussion section.

RESULTS AND DISCUSSION

Separating and Sorting Membrane-Bound Species Using Bilayer Extraction. In analogy to classic liquid−liquid extraction, we demonstrate a 2-D continuous extraction in SLBs by separating two lipid species: the glycolipid G_{M1}, and BODIPY DHPE, a phospholipid. These species were chosen because they have known affinities for the particular lipid phases we employ. For these experiments, we chose two stably coexistent lipid membrane phases. The l_d phase is 70 mol % POPC, 20 mol % PSM, and 10 mol % cholesterol. The l_o phase is 60 mol % PSM and 40 mol % cholesterol. The geometry of the two phases was patterned to facilitate continuous extraction and biomolecule sorting to different parts of the microfluidic chip following enrichment. The feed bilayer, containing the biomolecule mixture to sort, was chosen to match the l_d phase for maximum stability and compatibility. An illustration of the platform is in Figure 1A. Bilayer patterning was carried out using a combination

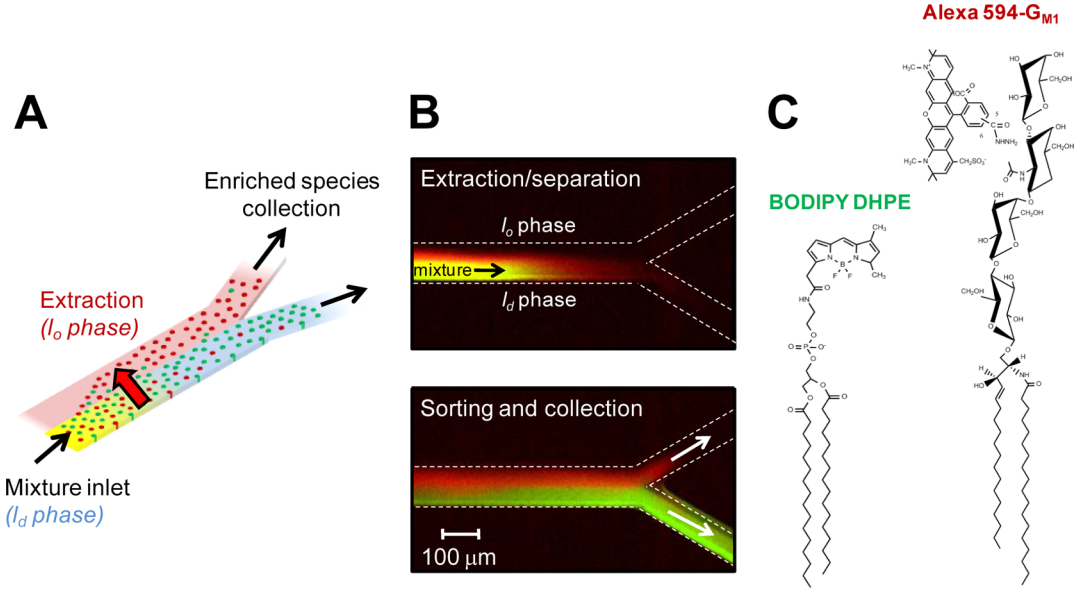

Figure 1. (A) Three-dimensional illustration of the two-phase supported lipid bilayer designed to separate and sort membrane biomolecules. The microfluidic device and glass support have been omitted for clarity. Laminar flow in a microfluidic device is used to create parallel stripes of coexistent lipid phases (l_d phase = blue, l_o phase = pink). The interface between the phases is contiguous, allowing membrane-bound molecules to partition into a preferred phase as they are transported down the main channel. The initial mixture is color-coded as red and green dots and is transported in the l_d phase. Red species are extracted into the l_o phase bilayer, causing the l_d phase to become more enriched in green species. (B) In the experiment, the mixture is BODIPY DHPE (green) and Alexa 594-G_{M1} (red) and appears yellow in the upper image. In these top-view images, the l_d phase was patterned in the bottom section, where yellow is dominant, while l_o phase is in the top half (initially devoid of any fluorophore). The species are transported to the right in the l_d phase membrane along the main channel. The red color ahead of the yellow plug is a small amount of Alexa 594-G_{M1} that moves slightly faster under bulk flow than BODIPY DHPE because it has a larger cross section. In the bottom image, the red Alexa 594-G_{M1} is extracted into the l_o phase, while BODIPY DHPE generally remains in the l_d phase. Separated fractions are split by the "Y" at the end of the channel. (C) The chemical structures of Alexa 594-G_{M1} and BODIPY DHPE.

dx.doi.org/10.1021/ac4006952 | *Anal. Chem.* 2013, 85, 6696−6702

of laminar flow and vesicle fusion techniques.[35] Details of constructing the patterned bilayer inside the microfluidic device are given in the Supporting Information.

After bilayer patterning, an applied hydrodynamic flow of the bulk solution in the microfluidic device provides a shear stress to drive the lipids in the membrane to move.[8,26,36] In this particular system, we characterized independently that the intrinsic mobility of biomolecules in the l_d phase is ~5 times greater than the mobility in the l_o phase using a fluorescence recovery after photobleaching technique.[35,37,38] Thus, most of the convection of biomolecules occurs in the l_d phase. When meeting the l_o phase, a biomolecule has the potential to be extracted depending on its chemical affinity. Figure 1B shows fluorescence images of continuous extraction in the patterned SLB platform.

To demonstrate separation, extraction, and sorting, two fluorescently labeled membrane biomolecules with differing propensities to partition into the two membrane phases were used. The fluorescent labels make it easy to track the biomolecules' positions in the device and quantify the extraction. We chose the glycolipid, G_{M1}, because it has established membrane partitioning behavior and serves as a typical marker for cell microdomains (lipids rafts). Since the acyl chain label in commercially available fluorescently labeled G_{M1} disrupts its native preference for ordered lipid phases in cell membranes,[33,39] we synthesized a head-labeled version, Alexa 594-G_{M1}.[15,35] We mixed Alexa 594-G_{M1} with another fluorescently labeled phospholipid, BODIPY DHPE, which generally prefers lipid disordered phases, such as those composed primarily of POPC.[35] The structures of both of these biomolecules are shown in Figure 1C.

In a first set of experiments, an approximately equimolar mixture of Alexa 594-G_{M1} (red fluorophore) and BODIPY DHPE (green fluorophore) was loaded into the device (1 mol % of each in the load bilayer formulation), Figure 1B. The mixture is yellow when the red and green false-color images are superimposed on each other (Figure 1B, top image). Figure 1B, bottom image, is a later snapshot of the continuous extraction, showing the preferential affinity of red Alexa 594-G_{M1} to the l_o phase, and the enrichment of the green BODIPY DHPE in the l_d phase. At the end of the channel a "Y" split directs the fractions to different areas of the chip for collection. A movie of the extraction and sorting process is provided in the Supporting Information. A control experiment without patterning is also shown there.

The exposure times during image acquisition for each channel (red or green) were set such that the starting intensities were nearly the same. The fluorescence intensity for each biomolecule in each phase varied linearly with concentration for the range of concentrations used here.[35] Because of these features, fluorescence intensity can be used to report concentration for these species to quantify the enrichment after the extraction process. To minimize photobleaching, samples were imaged every two minutes instead of continuously. Intensities were normalized to background fluorescence levels and minor corrections for vignetting were made, as described in the Supporting Information.

Extraction Efficiency: Theory and Analysis. On the basis of the design of this device, the extraction channel is analogous to a single stage extractor, operating in the 2-D plane of the bilayer. Due to practical kinetic limitations during experimental operation, the real performance of an extractor is often below what is predicted under equilibrium conditions. The real performance is quantified by calculating yield, Y, of a particular species in a particular lipid phase. A control volume in the 2-D membrane is shown in Figure 2. Initially, the entire control volume is devoid of any fluorescently labeled species. The yield in

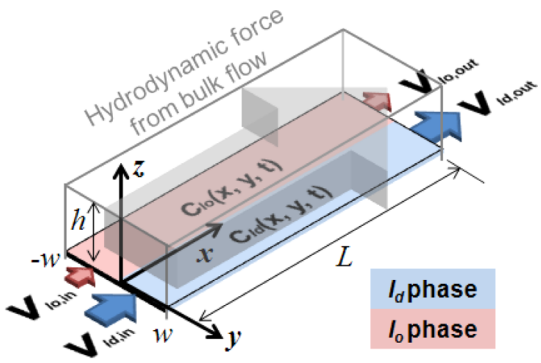

Figure 2. Two-dimensional two-phase bilayer control volume in a 3-D view of the microchannel with the parameters used in the data analysis. All parameters are defined in the text. Blue denotes the l_d phase, and pink denotes the l_o phase. The hydrodynamic force from the bulk flow (gray arrow) convects species in the lipid membrane.

phase i, $Y_i(t)$, is defined as the amount of species in phase i compared to the overall amount entering the control volume:

$$Y_i(t) = \frac{\alpha_{i,\text{out}}(t) + N_i(t)}{\alpha_{ld,\text{in}}(t) + \alpha_{lo,\text{in}}(t)} \quad (1)$$

Yield in these experiments is a function of time because the initial input (the mixture) is a discrete plug of material and the extracted amount is significantly influenced by the local concentration distribution of the species in the two phases. $\alpha_{i,\text{in}}$ and $\alpha_{i,\text{out}}$ are the cumulative material that has entered/left the control volume by the reporting time, respectively.

Material accumulation in each phase, $N_i(t)$, can be obtained directly by integrating fluorescence from the time-lapse micrographs. Cumulative material entering/exiting a particular phase in the control volume, $\alpha_i(t)$, is defined generally in eq 2, where $F_i(t)$ is the amount of material entering at $x = 0$ or exiting a phase i at $x = L$ in time:

$$\alpha_{i,\text{in or out}}(t) = \int_0^t F_{i,\text{in or out}}(t)\, dt \quad (2)$$

The equations that describe the amount of the material entering the l_o phase at $x = 0$ and exiting at $x = L$ in time are

$$F_{lo,\text{in}}(t) = \int_{y=-w}^{y=0} v(0, y)\cdot C(0, y, t)\, dy \quad (3)$$

$$F_{lo,\text{out}}(t) = \int_{y=-w}^{y=0} v(L, y)\cdot C(L, y, t)\, dy \quad (4)$$

where $v(x,y)$ is the velocity of a species in the membrane and w is the width of the phase cross-section. Under conditions of fully developed bulk flow, the overall velocity profile in the planar membrane is a function of y only. The concentration profile across the bilayer can be obtained by measuring fluorescence intensity from experimental images. To calculate the yield, all that remains is to determine the velocity profile in the two-phase membrane.

Characterization of Convection Velocity Profile in a Two-Phase Coexistent Supported Bilayer. In this work, the convection of biomolecules in the supported bilayer is induced by the shear force resulting from bulk buffer flow inside the microchannel. Previous study of homogeneous (single lipid phase) bilayer systems has shown that when sheared in this manner, the upper monolayer of the SLB moves in the direction of the drag while the lower monolayer is approximately stationary.[40,41] These studies suggest that the lipid monolayer can be viewed as a 2-D

dx.doi.org/10.1021/ac4006952 | Anal. Chem. 2013, 85, 6696−6702

continuum and the flow velocity can be described by the continuity equation and Navier–Stokes equation for creeping flow in 2-D and assuming fully developed flow and negligible viscous forces and surface pressure gradients.

We build upon this work to describe the motion of biomolecules in a two-phase heterogeneous bilayer arranged in two stripes parallel with the bulk hydrodynamic flow. We have experimentally observed that there are three regions with distinct membrane compositions: a l_o phase region, a l_d phase region, and an interfacial transition region in-between.[35] Species present in these different bilayer environments possess different mobilities, and therefore velocities, when subjected to a shear force. The overall velocity profile in this system is approximated as a piece-wise function of the velocity profile in each phase and interfacial region:

$$v(y) = \begin{cases} \dfrac{\sigma_{\text{hydro}}(y)}{b_{lo}} e_x & \text{when } y < y_{Tlo} \text{ in the } l_o \text{ phase} \\ \dfrac{\sigma_{\text{hydro}}(y)}{b_{\text{trans}}} e_x & \text{when } y_{Tlo} < y < y_{Tld} \text{ in the transition zone} \\ \dfrac{\sigma_{\text{hydro}}(y)}{b_{ld}} e_x = \dfrac{5\sigma_{\text{hydro}}(y)}{b_{lo}} e_x & \text{when } y > y_{Tld} \text{ in } l_d \text{ phase} \end{cases} \tag{5}$$

Here, y_{Tlo}, y_{Tld} are the locations of the boundaries of the transition zone between the l_o side and l_d side, respectively. b_{lo} = friction factor in the l_o phase, b_{trans} = friction factor in the transition zone between phases, and b_{ld} = friction factor in the l_d phase. The ratio for friction factor in l_o to l_d was ~5 for both BODIPY DHPE and Alexa 594-G_{M1} determined via a photobleaching technique, described in the Supporting Information. This ratio is substituted into the third part of eq 5 to reduce the number of parameters. $\sigma_{\text{hydro}}(y)$ is the shear force from hydrodynamic bulk fluid flow; the detailed expression for this parameter is described in the Supporting Information.

b_{trans} is difficult to define because the exact structure of the interfacial zone is unknown. However, since this region is small compared to the rest of the channel, we make the approximation that the velocity (and therefore b) varies linearly in this region. Thus, the velocity in this region can be rewritten to eliminate b_{trans} in eq 5 b as

$$\begin{aligned} v(y) &= \sigma_{\text{hydro}}\left(\frac{1}{b_{lo}} + \frac{y - y_{Tlo}}{y_{Tld} - y_{Tlo}}\left(\frac{1}{b_{ld}} - \frac{1}{b_{lo}}\right)\right)e_x \\ &= \sigma_{\text{hydro}}\left(\frac{1}{b_{lo}} + \frac{y - y_{Tlo}}{y_{Tld} - y_{Tlo}}\left(\frac{4}{b_{lo}}\right)\right)e_x \text{ when } y_{Tlo} < y < y_{Tld} \end{aligned} \tag{6}$$

The general velocity profile shape was visualized (Figure 3A, inset) using a photobleaching technique. The general shape is captured by our piece-wise model, so b_{lo} is the only parameter remaining to obtain $v(y)$.

Note that the photobleaching technique cannot be used directly to obtain b_{lo} in each extraction run because fluorescence intensity is being tracked as a proxy for concentration. Instead, an independent mass balance is used to determine the value of b_{lo} that corresponds to the experimental conditions of a particular run. To illustrate the mass balance process, we present the result for one experiment using the longest channel length, 710 μm, at 80 μL/min bulk flow rate (Figure 3B). This mass balance procedure is repeated for each experiment to obtain the best fit parameter for that experiment. The mass balance on the control volume is

$$\text{accumulation}(t) = \int_0^t \int_{-w}^{+w} [C(0, y, t)\cdot v(y)]_{\text{in}} - [C(L, y, t)\cdot v(y)]_{\text{out}}\, dy dt \tag{7}$$

Accumulation (left-hand side, LHS, of eq 7) can be obtained directly from time-lapse fluorescence micrographs and plotted as a function of time, as shown for Alexa 594-G_{M1} in Figure 3C (solid line). For the right-hand side, RHS, of eq 7, the concentrations, $C(0,y,t)$ and $C(L,y,t)$, are obtained directly from the fluorescence micrographs at the inlet and outlet locations. At this point, the magnitude of $v(y)$ for the RHS of eq 7 is unknown, but the shape of the profile has been experimentally verified, as described above, and is given by eq 5. Because the flow is steady, $v(y)$ does not vary with x, so the values at the inlet and outlet on a particular streamline are the same, i.e., $v(y)_{\text{in}} = v(y)_{\text{out}}$. b_{lo} is determined by minimizing the difference between the LHS and RHS of eq 7 (solid vs dashed lines, Figure 3C). For Alexa 594-G_{M1} for this particular run, $b_{lo} = 3.0 \times 10^8$ Pa s/m. The red line in Figure 3B is the corresponding velocity profile for Alexa 594-G_{M1}. The same procedure is followed for BODIPY DHPE.

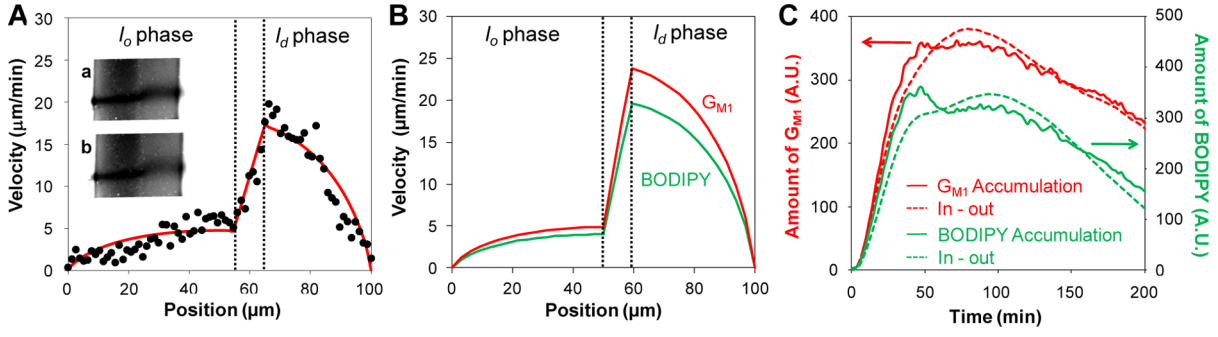

Figure 3. (A) Velocity profile obtained by photobleaching experiments (inset) to verify the shape of the profile and our model. Black data points are the velocities as a function of position across the channel, derived from the photobleached images, a and b, during 80 μL/min buffer flow rate. The red line is the best fit of the data by our model, eq 5. (B) Velocity profiles for Alexa 594-G_{M1} (solid red) and BODIPY DHPE (dashed green) determined for a particular extraction experiment using the 710 μm extraction channel. The interface region between each phase is defined by the black dashed lines. (C) The accumulation of species in the control volume (LHS eq 7) versus the difference between the inlet and outlet material flux for the control volume (RHS eq 7) in a representative run at 80 μL/min bulk flow rate for Alexa 594-G_{M1} (red), and BODIPY DHPE (green). These curves have been purposely offset by an arbitrary factor to separate the data. Velocity for each species was determined independently by minimizing the least-squares error between the LHS and RHS.

dx.doi.org/10.1021/ac4006952 | Anal. Chem. 2013, 85, 6696–6702

Table 1. Average Values Determined for b Based on Four Experiments

intermonolayer friction coefficient, b (Pa s/m)	BODIPY DHPE	Alexa 594-G_{M1}
l_o phase	$3.6 \pm 1.1 \times 10^8$	$2.8 \pm 0.8 \times 10^8$
l_d phase	$7.3 \pm 2.1 \times 10^7$	$5.6 \pm 1.7 \times 10^7$

The values for intermonolayer friction coefficients (b_i's) averaged over several experiments are shown in Table 1 and correspond well to values found in literature for similar bilayer phases.[27,42]

Extraction Performance. Once the velocity profile for an experimental run has been obtained, the yield of species can be calculated from eq 1. To quantify the enrichment of species in each phase, we measured the accumulation (yield) of both G_{M1} and BODIPY DHPE in the l_o phase as a function of the average residence time of a species in the device. The residence time, τ, is defined as the ratio of the channel length, L, to the average velocity of a species, $\hat{v}_{ld}$, in the l_d phase: $\tau = L/\hat{v}_{ld}$.

The residence time can be increased by increasing the length of the control volume or reducing the bulk flow rate. Here, we fix the bulk flow rate at 80 μL/min and varied the control volume lengths: 89, 355, and 710 μm. Each experiment is performed using the same channel geometry, bilayer compositions, and patterning, and a 50:50 starting mixture. Percent yields obtained from the experimental results for different residence times are shown in Figure 4. For the longest residence time, ~34% of the entering Alexa 594-G_{M1} is extracted into l_o phase during 200 min, while ~19% of the BODIPY DHPE is extracted.

The shape of the yield curve is influenced by the transport properties the biomolecule. If operated at equilibrium conditions, the extraction yields to the l_o phase are 66% and 38% for Alexa 594-G_{M1} and BODIPY DHPE, respectively, on the basis of previously measured equilibrium partition coefficients of 1.96 and 0.6.[35] Thus, even at the longest channel length investigated, equilibrium is not reached. Optimization of the channel dimensions, patterning, lipid phase selection, and process conditions can be carried out to approach equilibrium. One possibility is to lengthen the channel more, but this is only practical to a limit, beyond which diffusion becomes significant during laminar flow patterning and results in a less defined interface between lipid phases. Alternatively, decreasing the flow rate could allow partitioning to approach equilibrium. We found that halving the bulk flow rate increased the yield of G_{M1} to the lipid-ordered phase to ~40% at t = 200 min for L = 710 μm. The trade-off here is that the extraction takes longer.

Verification of Mass Balance Analysis Using Convection-Diffusion Model of Species Transport. To independently verify $v(y)$ and the intermonolayer friction factors (b_i's), we modeled the convection-diffusion for each species using COMSOL to simulate the extraction process. Parameter inputs were diffusivity, partitioning rates, and the b_i's (calculated as described above) to obtain the temporal concentration profiles in the control volume. Further details of the simulation are in the Supporting Information.

The b_i's determined by mass balance and used in the simulation predicted concentration profiles that closely matched experimental profiles (Figure S5), especially for shorter channel lengths. Other values shifted the elution time of the plug forward or backward because b directly impacts the velocity of the species in the bilayer. The shape of the velocity profile is also critical

Species	L (μm)	τ (min)	Yield in l_o phase (%)
Alexa – G_{M1}	89	4.7	26 ± 5
	355	19	28 ± 1
	710	37	34 ± 2
BODIPY DHPE	89	6.2	10 ± 4
	355	25	13 ± 3
	710	50	19 ± 3

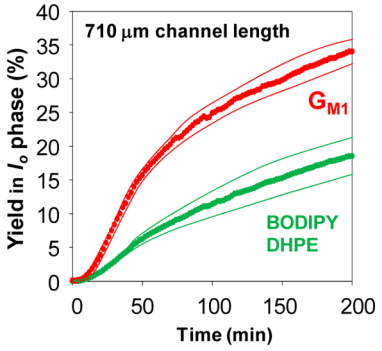

Figure 4. (Left) Yield of species to the l_o phase at various residence times, τ. The buffer flow rate was constant at 80 μL/min, but the length of the channel, L, was varied. These yields correspond to total experimental time, t = 200 min of collection. (Right) The accumulated yield of species in the l_o phase normalized by the total amount that has entered the control volume for L = 710 μm. These data are averaged over 4 experiments at the same conditions. The thin lines bounding the data points are the standard deviation of the data.

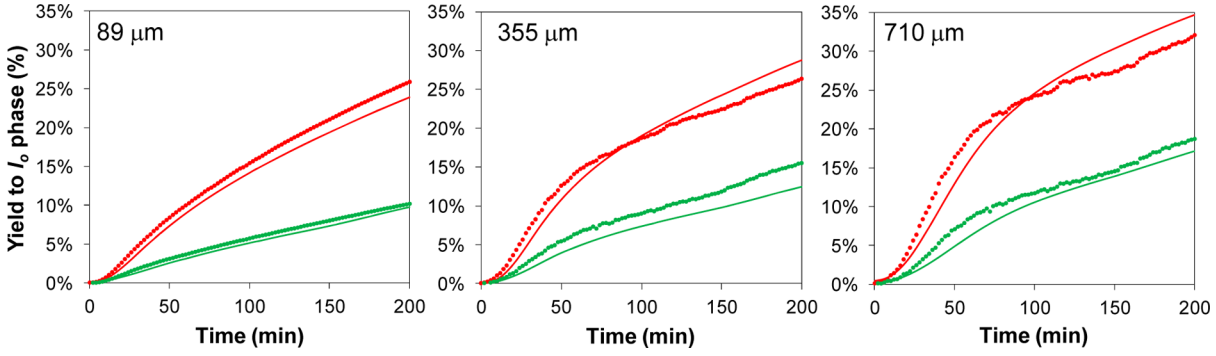

Figure 5. Comparison of yield of each species to the l_o phase for various channel lengths, as determined by experiment (points) and the model (lines) for Alexa 594-G_{M1} (red) and BODIPY DHPE (green).

dx.doi.org/10.1021/ac4006952 | Anal. Chem. 2013, 85, 6696–6702

to accurate modeling of the extraction. Inputting, for example, a uniform (average) velocity in each lipid phase across the channel (a step function velocity profile) with constant averaged b_i's was unable to capture the experimental concentration profiles.

When simulating the extraction for longer channel lengths, deviations grew between the experimental output concentration profiles and the model predictions (Figure S5). However, these deviations appear to have only a small effect on the predicted yield curve of an extracted species to the l_o phase up to the time of collection at t = 200 min, as seen in Figure 5.

Deviations between experimental results and simulation may result if the experimental velocity profile is not fully developed. We confirmed via photobleaching experiments that the flow is fully developed. Another explanation is that additional experimental dispersive effects that are not accounted for in the model become compounded as the channel lengthens. These effects may include patterning defects that disrupt the flow slightly and/or result in immobilization of biomolecules. These effects may accumulate as the length of channel increases. Nonetheless, our basic simulation reasonably predicts the extraction in this device, verifying that the parameters used in the model are acceptable. This model can be used to predict the enrichment of other biomolecules in this and other two-phase systems, or in optimizing the design of extraction devices.

CONCLUSIONS

The SLB extractor platform described herein can spatially separate, enrich, and sort membrane-bound species on the basis of their affinity for a specific lipid phase. We created two coexistent lipid phases, in analogy to classic liquid−liquid extraction, but operating in a flat plane of the supported bilayer. We demonstrate that G_{M1}, a typical lipid microdomain marker, can be extracted to an ordered lipid phase and become enriched, relative to nonraft species. This new platform does not require detergent, secondary antibody labeling methods, or electric fields often used in other strategies to identify lipid microdomain residents. Additionally, since the phase locations can be patterned to direct the species to a collection area, characterization tools, such as mass spectroscopy and surface plasmon resonance, could be also integrated at the outlet of this platform to identify unknown species or combined with other downstream analytical assays.

The approach described here is currently being extended to separate and sort lipids and proteins with post-translational modifications, such as the addition of GPI anchors, sterols, and single saturated or unsaturated fatty acids. The platform is compatible with species derived from cell membranes, and creating supported bilayers from sections of cell membrane has recently become possible,[43,44] including a new technique developed by us that uses cell blebs.[45] In the future, this platform could be extended to separating and sorting transmembrane species by integrating an appropriate cushion beneath the bilayer to minimize protein−support interactions.[44] Finally, this platform may be useful not just for separating and facilitating the identification of membrane domain residents, but for characterizing how post-translational modifications, interactions with soluble species, or environmental conditions shift the affinity of species to a particular lipid phase.[46,47]

ASSOCIATED CONTENT

Supporting Information

Materials and suppliers, experimental setup and procedures, microfluidic device fabrication, supported bilayer preparation, characterization, data analysis, control experiments, and sorting movie. This material is available free of charge via the Internet at http://pubs.acs.org.

AUTHOR INFORMATION

Corresponding Author

*Phone: 607-255-4675. Fax: 607-255-9166. E-mail: sd386@cornell.edu.

Present Address

‡Department of Chemical Engineering, National Taiwan University, Taipei, Taiwan

Author Contributions

†These authors contributed equally to this work.

Notes

The authors declare no competing financial interest.

ACKNOWLEDGMENTS

We thank the National Science Foundation (EEC-0824381, CBET-1149452) and an Innovation Grant from the Institute for Biotechnology and Life Science Technologies at Cornell University for support. M.J.R. is a fellow in Flexible Electronics for Biological and Life Science Applications. This fellowship is supported by the IGERT Program of the NSF (DGE-0654112) administered by the Nanobiotechnology Center at Cornell. This work was performed in part at the Cornell NanoScale Facility, which is supported by the NSF (ECS-0335765).

REFERENCES

(1) Lundstrom, K. *Comb. Chem. High Throughput Screening* **2004**, *7*, 431.
(2) Loll, P. J. *J. Struct. Biol.* **2003**, *142*, 144.
(3) Sachs, J. N.; Engelman, D. M. *Annu. Rev. Biochem.* **2006**, *75*, 707.
(4) Sprenger, R. R.; Horrevoets, J. G. *Proteomics* **2007**, *7*, 2895.
(5) Zheng, Y. Z.; Foster, L. J. *Proteomics* **2009**, *72*, 12.
(6) Joshi, M. K.; Dracheva, S.; Mukhopadhyay, A. K.; Bose, S.; Hendler, R. W. *Biochemistry* **1998**, *37*, 14463.
(7) Carlson, R. O.; Masco, D.; Brooker, G.; Spiegel, S. *J. Neurosci.* **1994**, *14*, 2272.
(8) Daniel, S.; Diaz, A. J.; Martinez, K. M.; Bench, B. J.; Albertorio, F.; Cremer, P. S. *J. Am. Chem. Soc.* **2007**, *129*, 8072.
(9) Weng, K. C.; Kanter, J. L.; Robinson, W. H.; Frank, C. W. *Colloids Surf., B* **2006**, *50*, 76.
(10) Groves, J. T.; Dustin, M. L. J. *Immunol. Methods* **2003**, *278*, 19.
(11) Diaz, A. J.; Albertorio, F.; Daniel, S.; Cremer, P. S. *Langmuir* **2008**, *24*, 6820.
(12) Wagner, M. L.; Tamm, L. K. *Biophys. J.* **2000**, *79*, 1400.
(13) Sumino, A.; Dewa, T.; Kondo, M.; Morii, T.; Hashimoto, H.; Gardiner, A. T.; Cogdell, R. J.; Nango, M. *Langmuir* **2011**, *27*, 1092.
(14) Chiantia, S.; Kahya, N.; Ries, J.; Schwille, P. *Biophys. J.* **2006**, *90*, 4500.
(15) Burns, A. R.; Frankel, D. J.; Buranda, T. *Biophys. J.* **2005**, *89*, 1081.
(16) Shreve, A. P.; Howland, M. C.; Sapuri-Butti, A. R.; Allen, T. W.; Parikh, A. N. *Langmuir* **2008**, *24*, 13250.
(17) Richter, R. P.; Brisson, A. R. *Biophys. J.* **2005**, *88*, 3422.
(18) Tokumasu, F.; Jin, A. J.; Feigenson, G. W.; Dvorak, J. A. *Biophys. J.* **2003**, *84*, 1.
(19) Ratto, T. V.; Longo, M. L. *Biophys. J.* **2002**, *83*, 3380.
(20) Lin, W. C.; Blanchette, C. D.; Ratto, T. V.; Longo, M. L. *Methods Mol. Biol.* **2007**, *400*, 503.
(21) Cheetham, M. R.; Bramble, J. P.; McMillan, D. G. G.; Krzeminski, L.; Han, X.; Johnson, B. R. G.; Bushby, R. J.; Olmsted, P. D.; Jeuken, L. J. C.; Marritt, S. J.; Butt, J. N.; Evans, S. D. *J. Am. Chem. Soc.* **2011**, *133*, 6521.
(22) Cremer, P. S.; Groves, J. T.; Kung, L. A.; Boxer, S. G. *Langmuir* **1999**, *15*, 3893.

(23) Stelzle, M.; Miehlich, R.; Sackmann, E. *Biophys. J.* **1992**, *63*, 1346.
(24) van Oudenaarden, A.; Boxer, S. G. *Science* **1999**, *285*, 1046.
(25) Nabika, H.; Takimoto, B.; Murakoshi, K. *Anal. Bioanal. Chem.* **2008**, *391*, 2497.
(26) Jonsson, P.; Beech, J. P.; Tegenfeldt, J. O.; Hook, F. *J. Am. Chem. Soc.* **2009**, *131*, 5294.
(27) Jönsson, P.; Gunnarsson, A.; Höök, F. *Anal. Chem.* **2010**, *83*, 604.
(28) Selvaraj, V.; Buttke, D. E.; Asano, A.; McElwee, J. L.; Wollf, C. A.; Nelson, J. L.; Klaus, A. V.; Hunnicutt, G. R.; Travis, A. J. *J. Androl.* **2007**, *28*, 588.
(29) Paulick, M. G.; Bertozzi, C. R. *Biochemistry* **2008**, *47*, 6991.
(30) Asano, A.; Nelson, J. L.; Zhang, S.; Travis, A. J. *Proteomics* **2010**, *10*, 3494.
(31) Legler, D. F.; Doucey, M.-A.; Schneider, P.; Chapatte, L.; Bender, F. C.; Bron, C. *FASEB J.* **2004**, DOI: DOI: 10.1096/fj.03-1338fje.
(32) Dietrich, C.; Bagatolli, L. A.; Volovyk, Z. N.; Thompson, N. L.; Levi, M.; Jacobson, K.; Gratton, E. *Biophys. J.* **2001**, *80*, 1417.
(33) Dietrich, C.; Volovyk, Z. N.; Levi, M.; Thompson, N. L.; Jacobson, K. *Proc. Natl. Acad. Sci. U.S.A.* **2001**, *98*, 10642.
(34) Stottrup, B. L.; Veatch, S. L.; Keller, S. L. *Biophys. J.* **2004**, *86*, 2942.
(35) Chao, L.; Daniel, S. *J. Am. Chem. Soc.* **2011**, *133*, 15635.
(36) Graneli, A.; Yeykal, C. C.; Prasad, T. K.; Greene, E. C. *Langmuir* **2006**, *22*, 292.
(37) Axelrod, D.; Koppel, D. E.; Schlessinger, J.; Elson, E.; Webb, W. W. *Biophys. J.* **1976**, *16*, 1055.
(38) Soumpasis, D. M. *Biophys. J.* **1983**, *41*, 95.
(39) Selvaraj, V.; Asano, A.; Buttke, D. E.; McElwee, J. L.; Nelson, J. L.; Wollf, C. A.; Merdiushev, T.; Fornes, M. W.; Cohen, A. W.; Lisanti, M. P.; Rothblat, G. H.; Kopf, G. S.; Travis, A. J. *J. Cell. Physiol.* **2006**, *206*, 636.
(40) Jönsson, P.; Höök, F. *Langmuir* **2010**, *27*, 1430.
(41) Jönsson, P.; Beech, J. P.; Tegenfeldt, J. O.; Höök, F. *Langmuir* **2009**, *25*, 6279.
(42) Merkel, R.; Sackmann, E.; Evans, E. *J. Phys. (Paris)* **1989**, *50*, 1535.
(43) Simonsson, L.; Gunnarsson, A.; Wallin, P.; Jönsson, P.; Höök, F. *J. Am. Chem. Soc.* **2011**, *133*, 14027.
(44) Tanaka, M.; Rossetti, F. F.; Kaufmann, S. *Biointerphases* **2008**, *3*, FA12.
(45) Costello, D. A.; Hsia, C.-Y.; Millet, J. K.; Porri, T.; Daniel, S. *Langmuir* **2013**, *29*, 6409.
(46) Leventhal, I.; Lingwood, D.; Grzybek, M.; Coskun, U.; Simons, K. *Proc. Natl. Acad. Sci. U.S.A.* **2010**, *107*, 22050.
(47) Wong, W.; Schlichter, L. *J. Biol. Chem.* **2003**, *279*, 444.